ISSN 1063-7729, Astronomy Reports, 2012, Vol. 56, No. 7, pp. 536–552. © Pleiades Publishing, Ltd., 2012.
Original Russian Text © I.D. Litovchenko, O.S. Bayandina, A.V. Alakoz, I.E. Val'tss, G.M. Larionov, D.V. Mukha, A.S. Nabatov, A.A. Konovalenko, V.V. Zakharenko, E.V. Alekseev, V.S. Nikolaenko, V.F. Kulishenko, S.A. Odintsov, 2012, published in Astronomicheskii Zhurnal, 2012, Vol. 89, No. 7, pp. 593–610.

OH 1720-MHz Lines as Tracers of Bipolar Outflows in the Vicinity of Class I Methanol Masers

I. D. Litovchenko[1*], O. S. Bayandina[1,2], A. V. Alakoz[1], I. E. Val'tss[1,2], G. M. Larionov[1], D. V. Mukha[3], A. S. Nabatov[3], A. A. Konovalenko[3], V. V. Zakharenko[3], E. V. Alekseev[3], V. S. Nikolaenko[3], V. F. Kulishenko[3], and S. A. Odintsov[4]

[1]*Astro Space Center, Lebedev Physical Institute, Russian Academy of Sciences, Profsoyuznaya ul. 84/32, Moscow 117997, Russia*

[2]*Moscow State Pedagogical University, ul. Malaya Pirogovskaya, 1, str. 1, Moscow, 119991 Russia*

[3]*Institute of Radio Astronomy, National Academy of Sciences of Ukraine, Krasnoznamennaya ul. 4, Kharkov 61002 Ukraine*

[4]*National Space Facilities Control and Testing Center, Evpatoria, 97419 Crimea, Ukraine*

Received November 18, 2010; in final form, November 22, 2011

Abstract—A sample of Class I methanol masers (MMI) has been surveyed at 1720 MHz to search for possible associations between MMI and 1720-MHz OH masers, which should be formed by the same collisional pumping mechanism. If the model for methanol masers is correct, the sample should contain a statistically significant number of 1720-MHz OH masers at the positions of MMI. The observations were conducted on the 70-meter radio telescope of the National Academy of Sciences of Ukraine (NASU). The results show that ∼50% of 72 MMI are associated with OH emission at 1720 MHz. In many sources, strong absorption lines are also observed. In most cases, the OH (1720) lines are narrow (linewidths of <2 km/s) suggesting they may be maser lines. The OH column densities obtained from Gaussian fitting of these narrow OH lines are, on average, 1.5×10^{17} cm^{-2}. The H_2 density in the emitting medium reaches 10^7 cm^{-3} if the region of the OH (1720) emission has been subject to interaction with a bipolar-outflow front. This is sufficient to excite MMI, and the presence of narrow, possibly masing OH (1720) lines at the MMI velocities indicates the likely presence of shocks from bipolar outflows in the vicinity of the maser condensations, supporting models in which these molecules are collisionally pumped.

DOI: 10.1134/S1063772912060042

1. INTRODUCTION

OH (hydroxyl) was the first and CH_3OH (methanol) the last of ten molecules from which maser emission has been observed in space. To date, 12 951 OH masers [1], ∼1500 H_2O masers [2], ∼1000 CH_3OH masers [3, 4], ∼40 NH_3 masers [5], ∼20 SiO masers [6], 13 HC_3N masers [7], and 7 H_2CO masers [8] have been detected. Approximately 10 SiS, CH, and HCN masers have also been observed.

What they have in common and what distinguishes them depends strongly on the type of object in which these masers are formed. OH masers are observed in various sources. In stars, they are found only in one of four transitions of the hyperfine structure in the Λ doubling of the OH rotational levels. The frequency of this transition is 1612 MHz for the ground state of the molecule. In the interstellar medium (ISM), all four hyperfine Λ-doubling transitions are observed toward star-forming regions (SFRs) in early evolutionary stages, however detections are mostly in the main lines, OH (1665) and OH (1667), and only rarely in the satellite lines. For example, among 200 SFRs with emission in the main OH lines, only 11 emit at 1612 MHz and 12 at 1720 MHz [9].

Emission in the OH (1720) satellite line is more frequently observed in regions at interfaces between the fronts of supernova remnants (SNRs) and molecular clouds; in this case, the main lines are observed in absorption (see, e.g., [10]).

Methanol masers are divided into two classes (MMI and MMII). Like main-line OH masers, MMIs are observed toward SFRs. The association of MMI with various objects of the ISM is not obvious: they are most frequently not associated with objects typical of SFRs, such as ultra-compact HII regions (UC HIIs), IRAS sources, or OH masers (1665, 1667 MHz).

*E-mail: grosh@asc.rssi.ru

The presence of ultra-compact HII regions or IRAS sources stimulates the excitation of rotational levels of OH and methanol by far-infrared radiation, with the subsequent decay and OH (1665, 1667) and MMII maser emission at 6.7 GHz in the cascade of *A* methanol and 12.2 GHz in the cascade of *E* methanol. This is the long known and well developed radiative-collisional pumping mechanism (see [11] for OH, [12–14] for CH_3OH, as well as references therein).

Far from UC HIIs or IRAS sources, ensembles of molecules are not affected by external radiation, and the excitation and decay of the molecules must follow some other scheme. The MMI pumping is purely collisional, and comes about due to the natural state of dense clumps in the ISM and the structure of methanol energy levels [15]. The decay of excited states of molecules is accompanied by maser emission, mostly at 44 and 95 GHz in the cascade of *A* methanol and at 36 GHz in the cascade of *E* methanol. The pumping pf OH (1720) masers is also collisional, and is also provided by the interaction of an SNR shock front with dense clumps in the ISM [16].

Collisional pumping is sensitive to density variations in the medium. It is believed that MMI formation can be strongly influenced by bipolar outflows from either massive or low-mass young stars.

We can ask the question: can OH masers and MMI appear in the same condensations? In other words, can bipolar outflows influence the formation of OH (1720) masers, and can a supernova shock front crossing a condensation increase the probability of MMI origin?

The idea that OH can be pumped by bipolar outflows was suggested by Argon et al. [17], who detected a possibly new class of OH masers in the W3(OH) region toward the Turner–Welch protostellar object.

The possibility of shocks forming 1720-MHz OH masers has been considered in a number of studies of supernovae; see, e.g., [10, 18], as well as [19], and references therein.

A targeted search for OH (1720) emission lines toward MMI in molecular clouds without relationships to supernova remnants has never been conducted. Such an attempt has been undertaken only for Class II methanol masers, which are formed by collisional–radiative pumping. One hundred star-forming regions with MMIIs were observed at four OH-maser frequencies on the Nançay telescope (France) [20]. In spite of the fact that OH masers radiating in the 1665- and 1612-MHz lines were detected in 55% of cases, the number of 1720-MHz masers was insignificant, as was the case for the Southern sky survey [9]: they were detected in only 6% of cases. This can only mean that the role of emission from nearby protostars or ultra-compact HII regions is much more important than the role of collisions in MMII pumping. A similar situation cannot be observed for Class I methanol masers if their pumping (and the pumping for 1720-MHz OH masers) is purely collisional. The possible connection between MMI and 1720-MHz OH masers requires dedicated study.

The first observations linking MMI and OH (1720) masers appeared in 2008, when the detection of 95-GHz emission toward the SNR Kes 79 was reported in [21]. This result was not confirmed by 44-GHz Onsala observations [22] or observations at 95 GHz carried out on the 12-m Arizona telescope and at 44 GHz on the VLA (M.J. Claussen, private communication, and D.A. Frail, quoted in [23]). It was noted in [22] that an attempt had been made to detect 44-GHz methanol emission toward several known SNRs with 1720-MHz OH emission using the Onsala telescope, also with a negative result. Studies of the relationships between SNRs, OH (1720) masers, and MMI are of current importance, and continue on the VLA [24].

However, the optimal solution of these problems and a first step in investigating the relationship between MMI and OH (1720) maser emission is studies of complete samples of Class I methanol masers at 1720 MHz, aimed at obtaining reliable statistical estimates.

To test the hypothesis that the pumping of MMI is collisional, we obtained observations in the 1720-MHz OH line of a complete sample of MMI accessible to the 70-m Evapatoria telescope (Ukraine). If this model for methanol masers is correct, this sample should contain a statistically significant number of 1720-MHz OH masers at the MMI positions. If the number of OH masers is small, models in which the pumping of the methanol and OH molecules is primarily collisional must be revised.

2. OBSERVATIONS

The observations were conducted on the 70-m radio telescope of the National Space Facilities Control and Testing Center in Evpatoria (National Academy of Sciences of Ukraine) on June 15–29, 2010, at the rest frequency of the OH transition, 1720.530 MHz, toward the coordinates of the MMI.

We selected 132 objects having declinations $>-35°$ that are accessible for observations at Evpatoria from a complete catalog of Class I methanol masers. At the time of the observations, the MMI catalog contained 198 sources (see http://www.asc.rssi.ru/MMI).

The telescope beamwidth at 1720 MHz is 9′. As a spectrometer, we used an autocorrelator with a frequency resolution of 4.028 kHz (4096 channels with a total bandwidth of 16.5 MHz), or 0.7 km/s in radial velocity at 1720 MHz. The calibration was done using standard continuum sources (3C 380 and 3C 123) and known maser sources (W51 and W75), as well as a noise generator. The system noise temperature was 35 K. The integration time for each source was 45 min. The observations were carried out in an ON–OFF mode, with the OFF observations carried out for five minutes following each source at a position offset by 15′ shift in elevation.

We observes 111 sources of the 132 selected; 21 sources were not observed for technical reasons. Four observed sources were not included in the subsequent analysis (W51Met1,2,5, which were in the beam together with the source W51e1/e2 and were also observed on different days and at different times to monitor the interference conditions, and DR 21, which falls into the beam with DR 21-West); i.e., we will consider 107 sources below.

3. PROCESSING: DATA RECORDING AND DECODING

The spectra were recorded using a digital correlation spectrometer designed and manufactured at the Institute of Radio Astronomy (National Academy of Sciences of Ukraine). The spectrometer produces 8192-channel spectra in a 33-MHz bandwidth with a frequency resolution of 4 kHz in two polarization channels. The correlator output yields power spectra in each polarization channel together with the complex cross-correlation function required to determine the Stokes parameters.

In the preliminary reduction, we used a specially developed frequency scheme enabling analysis of the data fed from the spectral correlator and the ability to work with the 1720-MHz spectra: the frequency of the first and local oscillators were 1250 MHz and 510 MHz, respectively. Thus, after the second frequency conversion, the studied segment of the spectrum began from 1760 MHz with a reversed run of the frequency (an inverted band). Finally, the last frequency conversion was implemented by sampling at 66 MHz. This results in a second inversion of the band relative to the Nyquist rate of 33 MHz. Thus, the inversion frequency corresponds to 1727 MHz, and the zero video frequency should correspond to a sky frequency of 1594 MHz; in this case, the run of the frequency in the spectrum is normal (going from low to high values). Since we were interested in a restricted frequency band, we saved only the upper half of the spectrum (1710.5–1727 MHz), i.e., 4096 harmonics, on the disk. Each number from the digital correlator occupies 4 bytes, or 32 bits, of which the mantissa occupies 5 bits. Each file has a header (256 bytes) containing information on the parameters of the experiment. Decoding software written in C was developed for the preprocessing of the data. This program also carries out additional averaging of the spectra in a given time interval; during the data acquisition, the correlator has already averaged the spectra over a time interval of 0.1 s.

The subsequent processing for the 111 sources observed had several stages.

We first calculated indents in the channels for each source. We then subtracted the baseline using a very high degree polynomial, separately for each polarization, to remove all broadband interference. This produced a group of files that contains 132 double windows for all sources, available at http://www.asc.rssi.ru/Lit/LB/online1.pdf. Empty windows were left for unobserved sources. The X axis is the line-of-sight velocity in km/s, and the Y axis the flux density in Jy. The dashed line in each spectrum shows the velocity of the methanol maser emission peak at 44 GHz; the OH (1720) emission was expected at this velocity.

The spectra of four test sources (W51Met1, 2, 5, and DR 21) are presented in the online figures.

Typical comb-type interference is observed in the spectra: see, for example, the six spectra in the interval from 189.032+0.785 to 205.539–14.602 and a number of others in which the interference is obvious. Owing to the presence of such interference in the spectrum of interest for us, we were not able to further analyze the data for 26 sources. In addition, we have not included further the sources 122.015–7.072, 173.481+2.446, and 183.348–0.577, since the signals in their spectra are located not at the methanol velocity and are probably also artefacts.

We will now describe doubtful cases, for which spectra are given online. In some spectra, for example, those of 10.47+0.03, 18.89–0.47(EGO), and 23.43–0.19, a single interference peak is present; at the same time, a weak signal could be present in these spectra. These sources must be reobserved; at the present stage, we have eliminated them from our subsequent analysis. Similarly, the two sources 16.868–2.158 (L379IRS3) and 34.82+0.352 (Mol75) may require a longer signal integration time. We have likewise not included these sources in the subsequent analysis.

Thus, we have 72 spectra that are free of obvious interference. We consider the data obtained to be sufficiently reliable and suitable for further processing. In 27 sources, we observe neither emission nor absorption in the OH (1720) line at the velocity of the MMI emission at the noise level of (50–100) mJy. This corresponds to 38% of the 72 objects selected

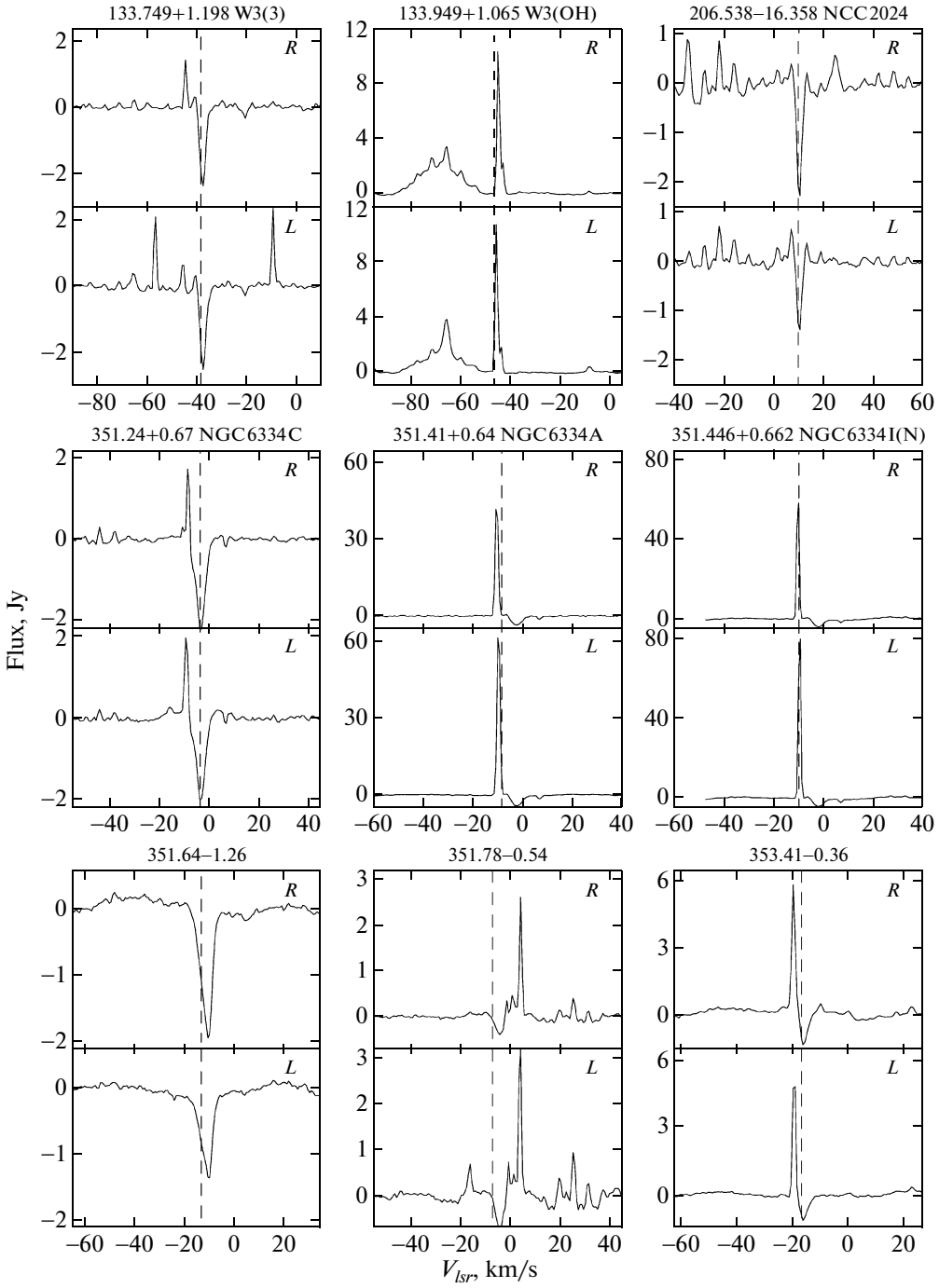

Fig. 1. 1720-MHz spectra measured toward Class I methanol masers using the Evpatoria 70-m telescope.

for the analysis. The list of these 27 MMI is given at http://www.asc.rssi.ru/Lit/LB/online2.pdf.

The next part of the processing was conducted in the European CLASS+GREG package. We fitted Gaussians to the spectra, and used the obtained fits to compare our flux densities S_ν at 1720 MHz and the flux densities for nine sources observed earlier on other telescopes (a list and information on the OH (1720) line parameters are given in Table 2). We derived a relationship for reducing the Evpatoria 70-m flux densities to the correct values:

$$S_{mod} = 2 \times S^{1.2}_{RT-70}.$$

In reality, these corrections must be introduced to flux densities $S_\nu > 10$ Jy, but we took it into ac-

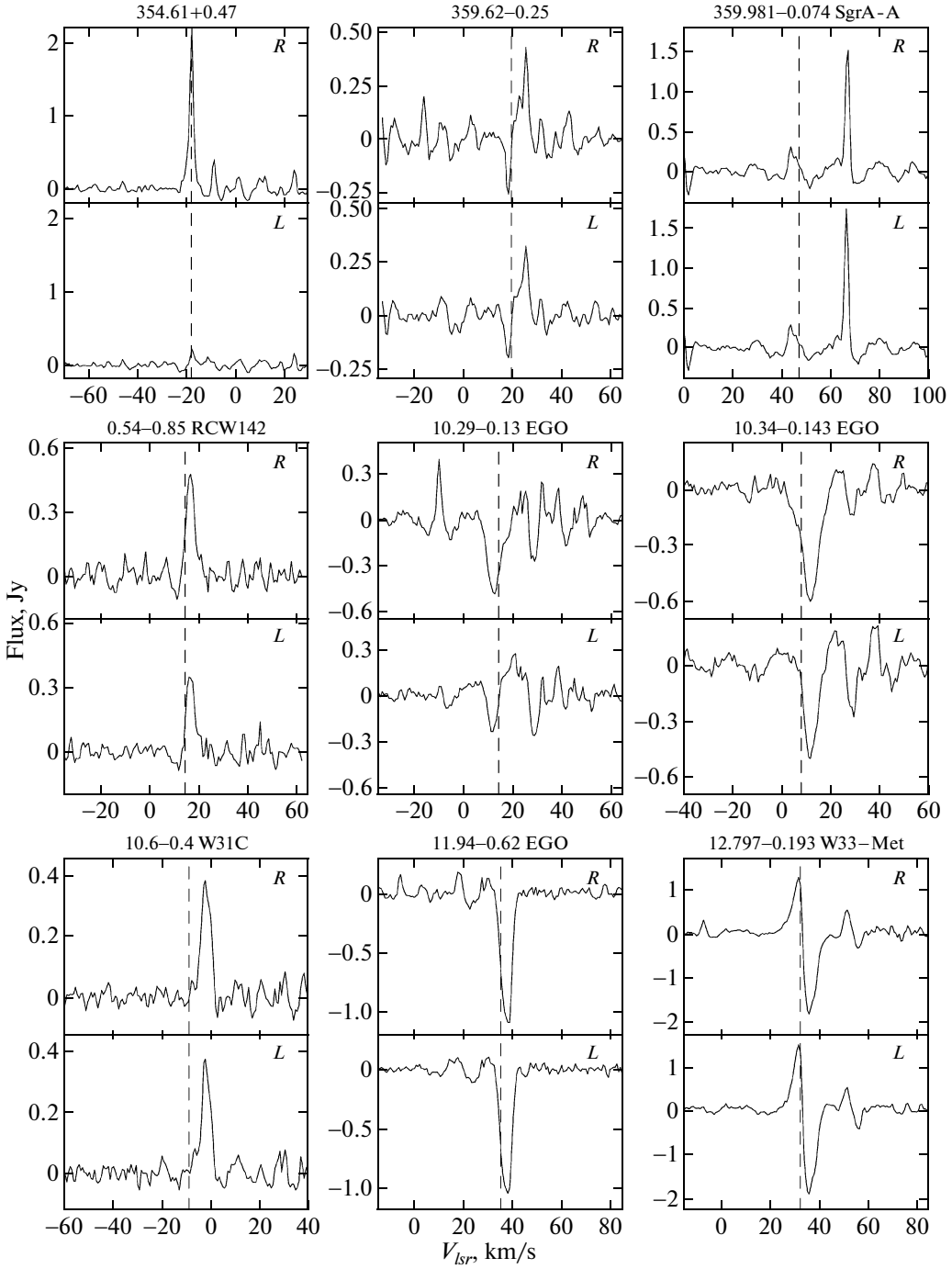

Fig. 1. (Contd.)

count for all sources. We updated the flux densities using these obtained corrections. The final 45 calibrated spectra for which we determined Gaussian line parameters are presented in the figure in the printed version of this paper, and are also available online at http://www.asc.rssi.ru/Lit/LB/online3.pdf. The results of the fits for the brightest lines in each spectrum are presented in Table 1. The full fits of all lines are listed in Table 1a in electronic form at http://www.asc.rssi.ru/Lit/LB/online4.pdf.

Table 2 contains a list of nine sources we used to calculate the corrections to the flux densities; the corresponding data and references are given.

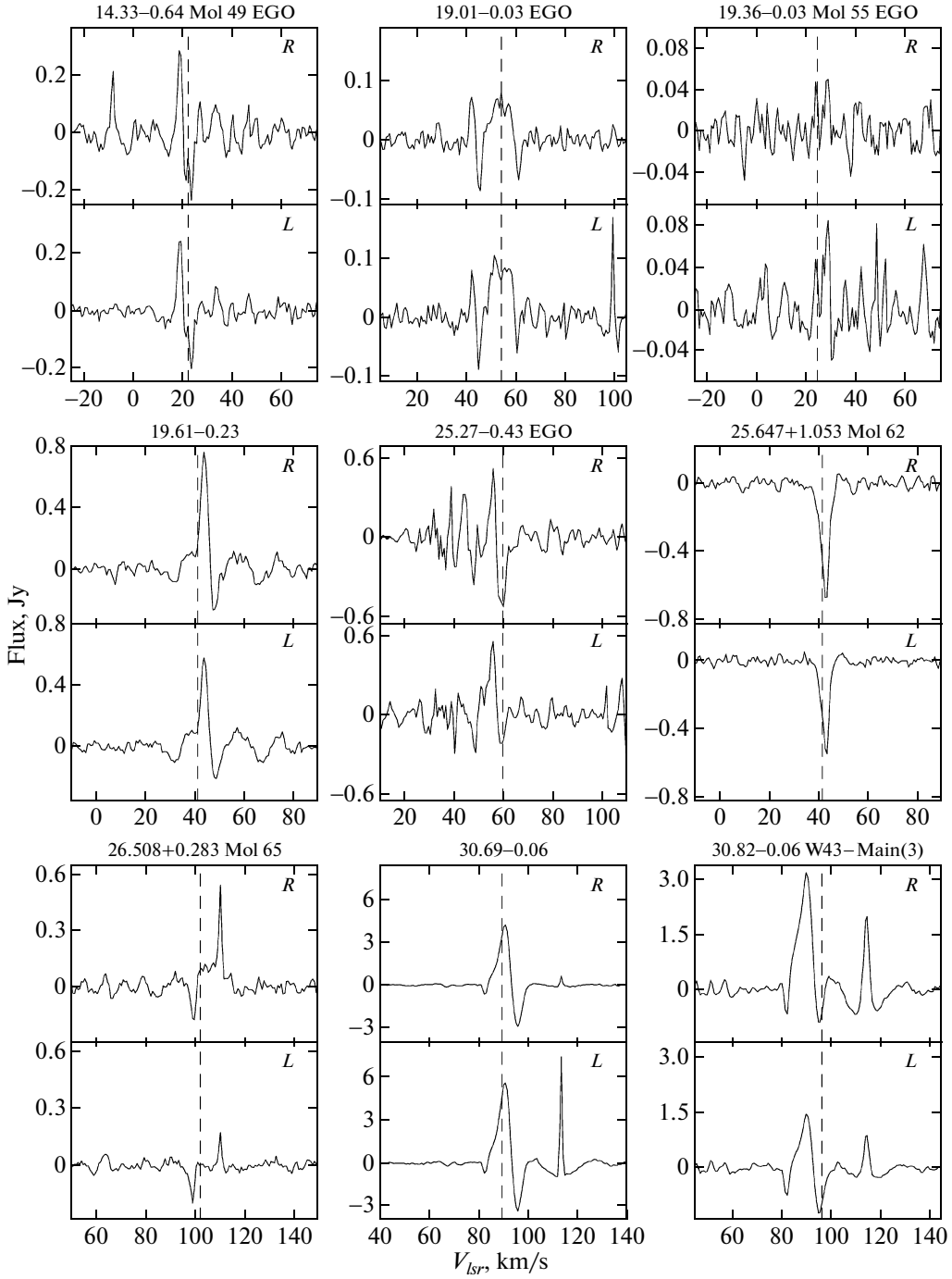

Fig. 1. (Contd.)

4. DISCUSSION

4.1. Properties of the Spectra and Comments on Individual Sources

We detected polarization in all the spectra; a strong line is present in only one polarization in 354.61+0.47 and 43.167+0.011 (W49N). Due to the complex situation with interference, we present spectra for a very broad velocity interval; the positions of the features in right- and left-circular polarization (RCP and LCP) in the figures coincide in velocity, possibly suggesting an absence of Zeeman splitting and so a relatively weak magnetic field in the studied regions. However, small differences in the velocities (as a rule, within the errors) are demonstrated in the Gaussian fitting of the line profiles (Table 1). This

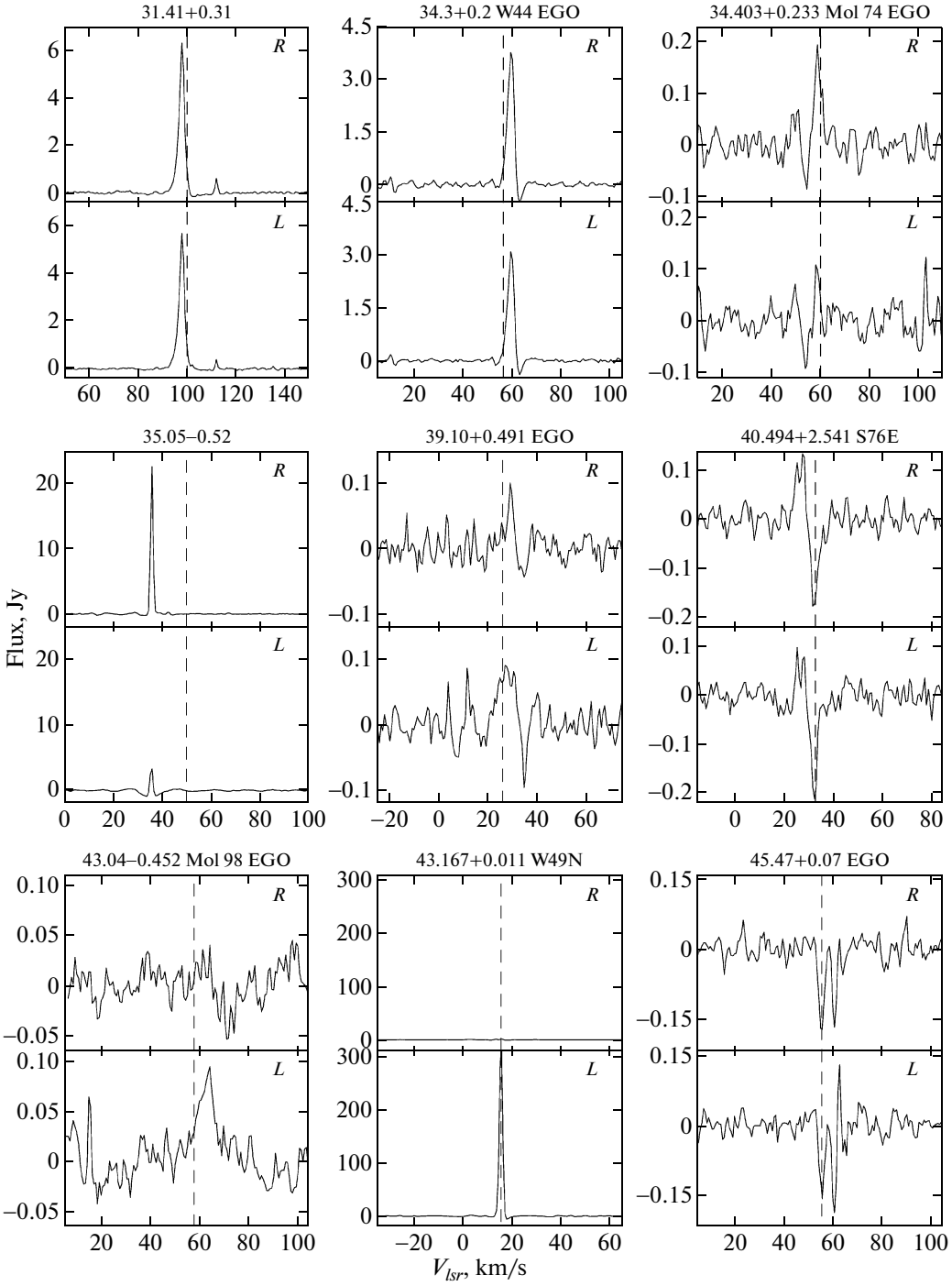

Fig. 1. (Contd.)

question requires more detailed study. We provide comments on individual sources below.

133.749+1.198 W3(3). Two emission features in LCP may be due to interference.

133.949+1.065 W3(OH). A broad feature between −50 and −90 km/s is an artefact due to comb-type interference. In this case, the interference does not fall into the studied segment of the spectrum, where both MMI emission and OH (1720) emission are present.

354.61+0.47. The spectrum is corrupted by typical interference with its edge at the MMI velocity. It cannot be ruled out that the feature observed in RCP is an artefact.

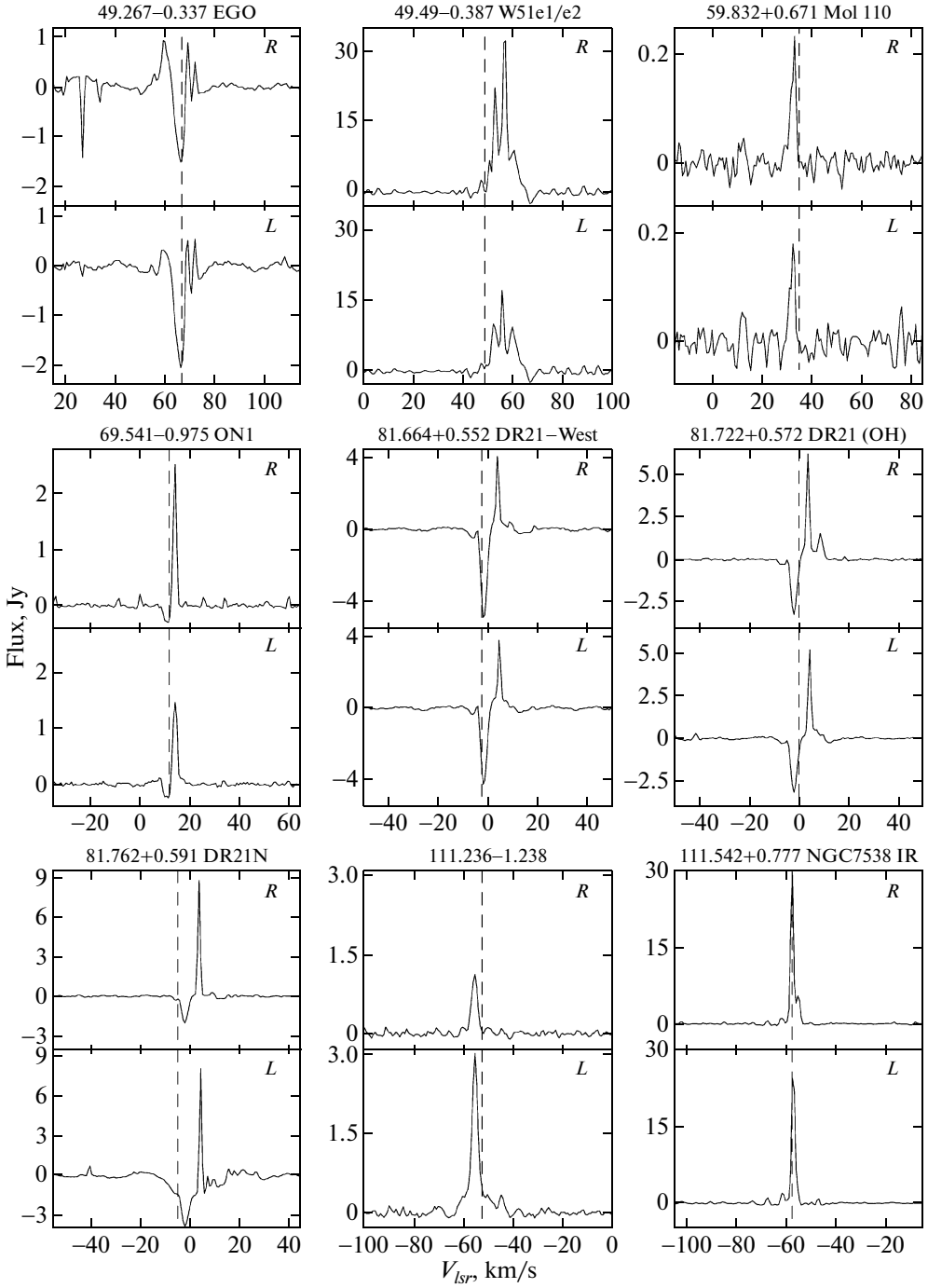

Fig. 1. (Contd.)

359.981−0.074 Sgr A-A. The observed features match the MMI velocity. However, strong OH (1720) lines were observed earlier in this source at −28.3, −8.4, and −6.8 km/s [25].

206.538−16.358. In the known source NGC 2024 (W12), in which absorption is observed in both the main and satellite OH lines [26], we see a possible weak emission feature in LCP at 1720 MHz.

30.69−0.06 and 30.82−0.06 (W43-Main (3)). These spectra contain interference with its maximum at about 115 km/s in both polarizations.

35.05−0.52. The velocity of the features observed at 1720 MHz does not fit the MMI velocity; the difference is approximately 15 km/s. This is probably due to interference in both polarizations, and the observed features are artefacts.

4.2. Analysis of the Emission and Absorption Features

The data of Table 1 indicate that, in ten cases, we observe only emission lines, in five only absorption lines, and in 30 both emission and absorption lines. In 20 of 32 sources (excluding 13 EGOs from the 45 objects, for which comments and analysis are given below), the emission lines are narrow, with linewidths of less than 2 km/s.

The flux densities in the emission lines observed in this survey are no lower than 100 mJy; they exceed 500 mJy for a considerable number of lines.

The profiles of the absorption lines in the emission–absorption spectra are asymmetric: features appear in both the blue and red part of the spectrum relative to the emission line. Features appear less frequently in the red part: in only three cases (NGC 6334C, 353.41–0.36, and W33-Met) are the absorption lines obvious and deep. In some other sources with mixed spectra, weaker absorption is visible in the red part of the spectrum. In 11 sources, absorption is observed in the blue part of the spectrum.

In all the mixed spectra, the emission lines are narrower than the absorption lines. The absorption linewidths are typical of the ISM, from 2 to 8 km/s.

The presence of absorption features in the spectra can be explained as follows. Since the methanol masers studied are associated with typical molecular clouds, the absorption lines could arise in the ordinary ISM of the spiral arms, like those observed in one of the first studies of OH absorption in the Galaxy [26]. In that survey, absorption lines were detected in all four OH Λ-doubling transitions toward 26 HII regions known by that time. The OH lines approximately reflected the distribution of these regions in the spiral arms, but their velocities differed from those of the nearby HII regions.

According to other observations, OH absorption lines can be tracers of bipolar outflows. A similar picture was observed in the well known nearby bipolar outflow in the dark cloud L1551 [27, 28]. In [27, 28], information is given only for the main lines, in which absorption lines with broad wings at the blue and red fronts of an outflow with a velocity range of up to ±30 km/s are observed, in addition to emission. The main-line OH spectra have a characteristic shape: with only emission lines observed toward its central part.

Note that Goss [26], Mirabel et al. [27], and Clark and Turner [28] hve emphasized that no discrete radio continuum sources have been detected toward OH sources.

The presence of methanol maser lines may indicate that the absorption features in the OH (1720) spectra are associated with absorption of the radio continuum emission of the surrounding medium, against the background of which the masing arises in a denser condensation at the central part of the source, demonstrated by the presence of maser emission there. The redshift and blueshift may characterize the motion of absorbing filaments relative to the maser condensation, driven by the bipolar outflow of material from a central protostar forming inside the maser condensation. The outflow could simultaneously amplify the effect of collisional pumping of the methanol and hydroxyl levels. In our observations, no broad wings in the OH (1720) absorption lines or appreciable shifts of these lines relative to the methanol velocity are observed. It is well known that the MMI velocities coincide with the velocities of the parent molecular clouds [29]. Therefore, a small blueshift or redshift of the OH (1720) absorption lines from the presumed central velocity of the condensation in which the MMI and OH (1720) emission is formed supports this hypothesis.

It is possible that we see different parts of a large molecular cloud falling within our beam, which may host different physical conditions (temperature and density); therefore, one part of the cloud could produce emission and another absorption. However, it is also possible that the physical conditions in the regions where the emission is generated are unstable, so that emission and absorption are formed in the same region. In this case, the OH (1720) and MMI regions coincide, since the velocities at which the MMI and OH (1720) emission/absorption regions are visible coincide within the width of MMI spectra [29].

The Evpatoria 70-m at 1720 MHz is 9′. Therefore, our observations do not necessarily imply spatial coincidence of the MMI and OH (1720) regions. Checking for spatial coincidence requires interferometric observations aimed at refining the positions, sizes, and brightness temperatures of both the OH (1720) and MMI masers. At the same time, we note that recent EVLA observations found no coincidence between the regions of 44-GHz MMI and OH (1720) emission toward the Center of the Galaxy [24].

4.3. Column Density of OH Molecules

Based on fitting the line profiles with standard formulas [26, 30], we have calculated the OH column density for the strongest feature in the spectrum separately in RCP and LCP and for lines in emission and in absorption.

The column density depends on the optical depth as

$$N_{\mathrm{OH}} = C_i T_{ex} \int \tau dv,$$

Table 1. Gaussian parameters of 1720-MHz OH lines observed toward Class I methanol masers in the survey

No.	Galactic coordinates	RA (B1950) RA (J2000)	Dec (B1950) Dec (J2000)	Polarization	Line number	$\int S_\nu dV$, Jy · km/s	V_{LSR}, km/s	Linewidth, km/s	S_{mod}, Jy	$\langle N_{\rm OH}\rangle$, 10^{16} cm^2
1	133.749+1.198	$02^h22^m06.1^s$	61°50′40″	RCP	1	1.6(0.3)	−44.57(0.09)	1.21(0.18)	1.23	0.9
	W3(3)	$02^h25^m53.5^s$	62°04′10.7″		2	−5.8(0.4)	−37.71(0.08)	2.50(0.19)	−2.17	3.4
				LCP	1	2.9(0.4)	−56.69(0.07)	1.06(0.19)	2.54	1.7
					2	−6.9(2.6)	−37.58(0.34)	2.81(0.74)	−2.30	4.1
2	133.949+1.065	02 23 17.3	61 38 58	RCP	1	13.7(1.4)	−44.70(0.06)	1.17(0.14)	10.98	81.0
	W3(OH)	02 27 4.62	61 52 25.6							
				LCP	1	13.5(1.1)	−44.70(0.05)	1.15(0.10)	11.02	80.0
3	206.538−16.358	05 39 11.4	−01 55 59	RCP	1	−6.12(0.29)	10.31(0.05)	2.28(0.12)	−2.521	3.6
	NGC 2024	05 41 42.86	−01 54 33.6							
				LCP	1	0.28(0.10)	7.25(0.13)	0.71(4.81)	0.37	0.2
					2	−4.46(0.21)	10.28(0.06)	2.43(0.14)	−1.72	2.6
4	351.24+0.67	17 16 54.51	−35 51 58.0	RCP	1	2.67(0.704)	−8.25(0.09)	1.11(0.31)	2.26	1.6
	NGC 6334-C	17 20 15.75	−35 54 58.1		2	−9.66(1.875)	−3.35(0.51)	6.37(1.60)	−1.43	5.7
	DDG 25			LCP	1	3.62(0.704)	−9.01(0.09)	1.59(0.25)	2.14	2.1
					2	−4.57(2.035)	−3.03(0.24)	3.19(0.76)	−1.35	2.7
5	351.41+0.64	17 17 32.2	−35 44 04	RCP	1	58.14(0.29)	−10.29(0.00)	1.28(0.01)	42.68	35.0
	NGC 6334A	17 20 53.24	−35 47 01.4		2	−8.69(0.31)	−2.19(0.07)	4.35(0.16)	−1.87	5.2
				LCP	1	81.76(0.30)	−9.59(0.00)	1.27(0.01)	60.65	49.0
					2	−10.07(0.31)	−2.06(0.07)	4.48(0.16)	−2.11	6.0
6	351.446+0.662	17 17 33.0	−35 42 04	RCP	1	64.90(0.51)	−10.30(0.00)	1.04(0.01)	58.78	39.0
	NGC 6334 I(N)	17 20 53.98	−35 45 01.3		2	−9.50(0.58)	−1.81(0.13)	4.56(0.32)	−1.96	5.6
				LCP	1	88.85(0.56)	−9.60(0.00)	1.02(0.01)	82.07	53.0
					2	−10.08(0.66)	−1.79(0.15)	4.74(0.36)	−2.00	6.0
7	351.64−1.26	17 25 55.00	−36 37 48.0	RCP	1	−9.86(0.29)	−10.80(0.07)	4.99(0.18)	−1.86	5.9
		17 29 17.9	−36 40 09.2							
				LCP	1	−6.40(0.34)	−10.86(0.14)	5.13(0.32)	−1.17	3.8
8	351.78−0.54	17 23 20.67	−36 06 45.4	RCP	1	−1.74(0.65)	−4.23(0.75)	3.77(1.56)	−0.43	1.0
		17 26 42.57	−36 09 17.7		2	2.93(0.47)	4.56(0.10)	1.06(0.16)	2.61	1.7
				LCP	1	−2.73(1.42)	−3.99(1.02)	3.85(2.21)	−0.67	1.6
					2	3.31(1.01)	4.26(0.16)	1.00(0.56)	3.10	2.0
9	353.41−0.36	17 27 07.00	−34 39 41.0	RCP	1	8.66(0.25)	−19.39(0.02)	1.43(0.05)	5.71	5.1
		17 30 26.48	−34 41 57.1		2	−2.91(0.24)	−15.59(0.12)	2.56(0.25)	−1.07	1.7
				LCP	1	7.70(0.20)	−19.14(0.01)	1.14(0.04)	6.33	4.6
					2	−2.69(0.22)	−15.68(0.13)	3.53(0.37)	−0.72	1.6
10	354.61+0.47	17 27 00.00	−33 11 38.0	RCP	1	4.17(0.154)	−17.70(0.03)	1.93(0.09)	2.034	2.4
		17 30 17.02	−33 13 54.7							
11	359.62−0.25	17 42 30.00	−29 22 31.0	RCP	1	−0.52(0.64)	18.24(0.87)	1.95(1.16)	−0.25	0.3
		17 45 41.22	−29 23 40.5		2	0.87(0.13)	25.45(0.14)	1.92(0.33)	0.43	0.5
				LCP	1	−0.55(0.14)	18.13(0.20)	2.41(0.44)	−0.21	0.3
					2	0.63(0.17)	25.48(0.14)	2.15(0.37)	0.28	0.4

Table 1. (Contd.)

No.	Galactic coordinates	RA (B1950) RA (J2000)	Dec (B1950) Dec (J2000)	Polarization	Line number	$\int S_\nu dV$, Jy · km/s	V_{LSR}, km/s	Linewidth, km/s	S_{mod}, Jy	$\langle N_{\rm OH}\rangle$, 10^{16} cm^2
12	359.981−0.074	17 42 41.3	−28 58 18	RCP	1	3.08(0.11)	66.76(0.03)	1.78(0.07)	1.63	1.8
	SgrA-A	17 45 51.9	−28 59 26.7							
				LCP	1	2.95(0.22)	66.35(0.06)	1.73(0.15)	1.60	1.7
13	0.54−0.85	17 47 04.1	−28 54 01	RCP	1	2.29(0.09)	16.82(0.08)	4.12(0.20)	0.52	1.4
	RCW 142	17 50 14.63	−28 54 50.6							
				LCP	1	2.14(0.41)	17.33(0.53)	5.49(1.55)	0.37	1.3
14	10.29−0.13	18 05 57.9	−20 06 26	RCP	1	−4.29(3.73)	12.16(2.36)	6.73(3.05)	−0.60	2.5
	EGO	18 08 49.528			2	1.14(0.16)	24.37(0.70)	6.12(0.70)	0.18	0.7
				LCP	1	−4.75(2.55)	12.26(0.65)	7.91(2.26)	−0.56	2.8
					2	0.21(0.37)	25.52(1.57)	1.90(4.39)	0.10	0.1
15	10.34−0.143	18 06 10.93	−20 04 08.5	RCP	1	−3.63(1.19)	11.96(0.62)	6.56(1.39)	−0.52	2.2
	EGO	18 09 00.0	−20 03 35.0		2	0.56(0.36)	23.21(1.58)	4.42(2.48)	0.12	0.3
				LCP	1	−4.21(1.03)	12.19(0.42)	7.75(1.43)	−0.51	2.5
16	10.6−0.4	18 07 30.5	−19 56 28	RCP	1	1.694(0.09)	−1.91(0.11)	4.31(0.25)	0.37	1.0
	W31C	18 10 28.4	−19 55 48.7							
				LCP	1	1.634(0.30)	−1.72(0.36)	4.09(0.89)	0.38	1.0
17	11.94−0.62	18 11 04.4	−18 54 20	RCP	1	3.34(1.17)	29.71(2.58)	4.21(3.37)	0.22	2.0
	EGO	18 14 00.92	−18 53 25.2		2	−5.59(1.00)	37.50(0.10)	4.75(0.38)	−1.11	3.3
				LCP	1	0.92(0.10)	30.34(0.70)	4.85(0.70)	0.18	0.6
					2	−4.28(0.13)	37.33(0.70)	4.25(0.70)	−0.95	2.5
18	12.797−0.193	18 11 15.7	−17 56 53	RCP	1	7.10(1.93)	32.07(0.13)	3.64(0.53)	1.83	4.2
	W33-Met	18 14 10.99	−17 55 57.4		2	−16.17(2.02)	36.00(0.43)	7.09(0.63)	−2.14	9.5
				LCP	1	6.64(0.16)	32.05(0.01)	3.48(0.09)	1.80	3.9
					2	−15.90(0.22)	36.03(0.02)	6.99(0.09)	−2.14	9.4
19	14.33−0.64	18 16 00.80	−16 49 06.0	RCP	1	−0.07(0.08)	23.98(0.48)	0.70(5.13)	−0.09	0.04
	Mol 49	18 18 54.61	−16 47 49.7		2	0.84(0.16)	19.12(0.22)	2.20(0.49)	0.36	0.5
	EGO			LCP	1	0.56(0.06)	19.15(0.11)	1.92(0.21)	0.28	0.3
					2	−0.58(0.27)	23.81(0.34)	3.48(1.09)	−0.16	0.04
20	19.01−0.03	18 22 56.52	−12 24 32	RCP	1	0.16(0.04)	42.36(0.25)	2.00(0.51)	0.08	0.1
	EGO	18 25 44.8	−12 22 45.8		2	−0.17(0.04)	45.35(0.20)	1.73(0.39)	−0.09	0.1
				LCP	1	0.48(0.12)	51.78(0.51)	4.51(1.14)	0.10	0.3
					2	−0.12(0.04)	45.21(0.25)	1.29(0.46)	−0.09	0.1
21	19.36−0.03	18 23 37.9	−12 05 46.1	RCP	1	0.05(0.02)	24.68(0.36)	0.74(9.29)	0.06	0.03
	Mol 55	18 26 25.8	−12 03 56.9							
	EGO			LCP	1	0.15(0.03)	28.92(0.27)	1.94(0.51)	0.07	0.1
22	19.61−0.23	18 24 50.3	−11 58 34	RCP	1	2.65(1.09)	44.10(0.29)	3.49(0.75)	0.71	1.6
		18 27 38.05	−11 56 39.5		2	−0.52(0.67)	47.77(0.64)	2.77(1.38)	−0.18	0.3
				LCP	1	2.56(0.10)	44.05(0.70)	3.42(0.70)	0.70	1.5
					2	−0.84(0.08)	48.84(0.70)	5.00(0.70)	−0.16	0.5
23	25.27−0.43	18 36 15	−07 07 31.7	RCP	1	1.63(0.98)	56.01(0.16)	2.23(0.69)	0.69	1.0
	EGO	18 38 56.9	−07 00 48.0		2	−2.59(1.03)	58.94(0.86)	4.70(1.66)	−0.52	1.5
				LCP	1	1.45(0.32)	55.90(0.70)	2.54(0.70)	0.54	0.9
					2	−0.73(0.27)	58.74(0.70)	3.30(0.70)	−0.21	0.4

Table 1. (Contd.)

No.	Galactic coordinates	RA (B1950) RA (J2000)	Dec (B1950) Dec (J2000)	Polarization	Line number	$\int S_\nu dV$, Jy · km/s	V_{LSR}, km/s	Linewidth, km/s	S_{mod}, Jy	$\langle N_{\rm OH}\rangle$, 10^{16} cm^2
24	25.647+1.053	18 31 39.15	−06 02 07.7	RCP	1	−1.87(0.16)	46.03(0.10)	2.45(0.24)	−0.72	1.1
	Mol 62	18 34 19.8	−05 59 44							
				LCP	1	−1.98(0.18)	43.20(0.15)	3.33(0.32)	−0.56	1.2
25	26.508+0.283	18 36 0.15	−05 37 47.5	RCP	1	−0.85(0.16)	99.59(0.25)	3.23(0.76)	−0.25	0.5
	Mol 65	18 38 40.3	−05 35 06		2	0.51(0.08)	110.54(0.10)	1.16(0.20)	0.41	0.3
				LCP	1	−0.30(0.23)	99.43(0.16)	1.59(0.59)	−0.18	0.2
					2	0.20(0.06)	110.50(0.14)	1.10(0.29)	0.17	0.1
26	30.69−0.06	18 44 58.9	−02 04 27	RCP	1	−19.90(0.66)	95.84(0.70)	4.47(0.70)	−4.18	12.0
		18 47 34.93	−02 01 06		2	15.51(0.65)	90.58(0.70)	4.08(0.70)	3.57	9.2
				LCP	1	−51.25(48.09)	93.90(1.64)	6.48(1.09)	−7.43	30.0
					2	49.59(48.95)	91.68(0.94)	5.35(1.04)	8.70	29.0
27	30.82−0.06	18 45 11.0	−01 57 57	RCP	1	−8.27(0.38)	95.70(0.70)	4.27(0.70)	−1.82	4.9
	W43-Main(3)	18 47 46.9	−01 54 35.2		2	8.63(0.40)	114.88(0.70)	3.52(0.70)	2.30	5.1
				LCP	1	−7.80(4.68)	95.35(0.31)	4.35(0.87)	−1.68	4.6
					2	4.66(0.36)	114.85(0.11)	3.17(0.31)	1.38	2.8
28	31.41+0.31	18 44 59.1	−01 16 10.66	RCP	1	15.55(0.17)	98.22(0.00)	2.35(0.03)	6.23	9.2
		18 47 34.21	−01 12 49.7							
				LCP	1	13.73(2.38)	98.26(0.02)	2.28(0.09)	5.65	8.1
29	34.3+0.2	18 50 46.2	01 11 12	RCP	1	22.46(2.32)	60.33(0.09)	3.86(0.21)	5.47	13.0
	W44	18 53 18.51	01 14 57.6		2	−12.40(2.00)	61.55(0.33)	3.56(0.28)	−3.27	7.4
	EGO			LCP	1	18.70(4.02)	60.27(0.27)	4.01(0.18)	4.38	11.0
					2	−8.40(5.62)	61.79(0.18)	3.16(0.24)	−2.50	5.0
30	34.403+0.233	18 50 45.29	01 21 09.5	RCP	1	−0.52(0.11)	53.23(0.36)	3.28(0.68)	−0.15	0.3
	Mol 74	18 53 17.4	01 24 55							
	EGO			LCP	1	−0.11(0.06)	54.30(0.47)	1.68(1.00)	−0.06	0.07
					2	0.30(0.07)	59.07(0.25)	2.20(0.54)	0.13	0.2
31	35.05−0.52	18 54 37.1	01 35 01	RCP	1	−1.94(0.16)	32.83(0.19)	4.72(0.44)	−0.39	1.1
		18 58 08.96	01 39 02.9		2	28.34(0.20)	35.89(0.00)	1.16(0.01)	22.88	17.0
				LCP	1	−0.96(0.10)	32.24(0.19)	4.32(0.63)	−0.21	0.6
					2	5.49(0.11)	35.69(0.01)	1.26(0.02)	4.11	3.3
32	39.10+0.491	18 58 30.83	05 38 25.8	RCP	1	−0.43(0.18)	34.97(0.76)	3.91(1.48)	−0.10	0.3
	EGO	19 00 58.1	05 42 44.0							
				LCP	1	−0.76(0.11)	34.68(0.31)	4.99(0.86)	−0.14	0.5
33	40.494+2.541	18 53 46	07 49 16	RCP	1	−0.83(0.11)	33.03(0.18)	3.74(0.55)	−0.21	0.5
	S76E	18 56 10.74	07 53 14.1							
				LCP	1	−0.54(0.04)	32.86(0.09)	2.64(0.22)	−0.19	0.3
34	43.04−0.452	19 09 14.9	08 41 34.7	RCP	1	−0.10(0.03)	71.68(0.30)	1.61(0.57)	−0.06	0.06
	Mol 98	19 11 38.81	08 46 37.9							
	EGO			LCP	1	0.39(0.47)	63.29(0.94)	5.64(3.73)	0.07	0.2
35	43.167+0.011	19 07 49.8	09 01 17	RCP	1	8.88(4.39)	15.95(0.05)	1.82(0.22)	4.58	5.3
	W49N	19 10 13.31	09 06 14.3		2	−7.05(4.10)	17.04(0.70)	2.84(0.67)	−2.33	4.2
				LCP	1	473.88(2.68)	15.45(0.00)	1.51(0.01)	295.86	280.0
					2	−9.11(1.61)	17.50(0.20)	3.07(0.506)	−2.78	5.4

Table 1. (Contd.)

No.	Galactic coordinates	RA (B1950) RA (J2000)	Dec (B1950) Dec (J2000)	Polarization	Line number	$\int S_\nu dV$, Jy · km/s	V_{LSR}, km/s	Linewidth, km/s	S_{mod}, Jy	$\langle N_{\rm OH}\rangle$, 10^{16} cm^2
36	45.47+0.07	19 12 04.5	11 04 22.46	RCP	1	−0.54(0.12)	55.79(0.17)	2.56(0.43)	−0.20	0.3
	EGO	19 14 25.73	11 09 37.3							
				LCP	1	−0.59(0.086)	60.86(0.15)	2.00(0.32)	−0.28	0.4
37	49.267−0.337	19 20 48.95	14 14 22.2	RCP	1	1.93(0.34)	60.24(0.33)	3.42(0.66)	0.53	0.5
	EGO	19 23 06.7	14 20 13.0		2	−2.53(0.35)	66.59(0.26)	3.39(0.52)	−0.70	0.7
					3	0.89(0.27)	69.39(0.15)	1.32(0.32)	0.63	0.2
				LCP	1	1.91(0.29)	60.15(0.37)	4.15(0.64)	0.43	0.5
					2	−2.03(0.28)	66.64(0.23)	3.11(0.44)	−0.61	0.5
					3	0.86(0.24)	69.20(0.11)	1.26(0.36)	0.64	0.2
38	49.49−0.387	19 21 26.2	14 24 43	RCP	1	69.19(1.46)	59.97(0.02)	1.90(0.05)	34.25	41.0
	W51e1/e2	19 23 43.77	14 30 36.3		2	−6.03(6.17)	70.15(1.92)	3.19(3.40)	−1.78	3.6
				LCP	1	26.00(1.23)	59.13(0.03)	1.58(0.09)	15.47	15.0
					2	−6.06(3.66)	70.15(1.05)	3.11(1.93)	−1.83	3.6
39	59.832+0.671	19 38 52.6	23 57 35.8	RCP	1	0.50(0.03)	33.26(0.09)	2.38(0.20)	0.20	0.3
	Mol 110	19 40 59.3	24 04 39							
				LCP	1	0.38(0.04)	32.87(0.13)	2.42(0.29)	0.15	0.2
40	69.541−0.975	20 08 09.9	31 22 42	RCP	1	−0.54(0.06)	11.07(0.15)	2.52(0.32)	−0.20	0.3
	ON 1	20 10 09.05	31 31 37.3		2	3.80(0.08)	14.31(0.02)	1.50(0.04)	2.39	2.3
				LCP	1	−0.71(0.05)	11.30(0.12)	2.86(0.21)	−0.23	0.4
					2	3.04(0.07)	14.36(0.02)	1.96(0.04)	1.46	1.8
41	81.664+0.552	20 37 07.6	42 08 46	RCP	1	−17.27(0.80)	−1.47(0.02)	3.01(0.07)	−5.39	10.0
	DR 21-West	20 38 54.5	42 19 23.4		2	4.12(0.11)	3.98(0.01)	1.16(0.03)	3.35	2.4
				LCP	1	−18.08(1.16)	−1.50(0.04)	3.12(0.11)	−5.45	11.0
					2	3.82(0.14)	4.64(0.02)	1.13(0.05)	3.17	2.3
42	81.722+0.572	20 37 13.8	42 12 13	RCP	1	−10.91(0.51)	−1.56(0.70)	3.06(0.70)	−3.34	6.5
	DR 21(OH)	20 39 00.62	42 22 50.8		2	7.00(0.55)	3.95(0.70)	1.28(0.70)	5.14	4.2
				LCP	1	−11.42(0.52)	−1.56(0.05)	3.12(0.13)	−3.44	6.8
					2	6.78(0.33)	4.62(0.02)	1.29(0.05)	4.96	4.0
43	81.762+0.591	20 37 15.26	42 15 05.2	RCP	1	−5.59(0.45)	−1.71(0.11)	3.03(0.26)	−1.73	3.3
	DR 21N	20 39 02.0	42 25 43.0		2	10.30(0.28)	3.94(0.02)	1.13(0.03)	8.59	6.1
				LCP	1	−6.92(1.86)	−1.60(0.36)	3.10(0.72)	−2.10	4.1
					2	11.63(0.81)	4.59(0.04)	1.14(0.08)	9.61	6.9
44	111.236−1.238	23 15 08.7	59 12 25.2	RCP	1	4.55(0.47)	−55.27(0.01)	3.05(0.25)	1.40	2.7
		23 17 21.0	59 28 49.0							
				LCP	1	6.43(0.87)	−55.11(0.03)	2.53(0.17)	2.39	3.8
45	111.542+0.777	23 11 36.7	61 11 49	RCP	1	33.66(0.23)	−57.36(0.00)	1.18(0.01)	26.77	20.0
	NGC 7538 IR	23 13 45.34	61 28 09.7							
				LCP	1	36.16(0.22)	−56.86(0.00)	1.42(0.01)	24.00	21.0

Table 2. Class I methanol masers with previously observed 1720-MHz OH lines used to correct the flux densities

No.	Galactic coordinates	Source name	RA J2000	Dec J2000	OH (1720) S_ν and V_{LSR}, Jy and km/s
2	133.949+1.065	W3(OH)	$02^h27^m4.62^s$	61°52′25.6″	8.32R; −44.33[1]
					10.40L; 45.56[1]
5	351.41+0.64	NGC 6334A			46; −11.26[2]
		NGC 6334-F	17 20 53.39	−35 47 01.6	46; −10.35[2]
		NGC 6334N(orth)			22; −10[3]
					86L; −10.2[4]
					60.31R; −10.59[1]
					83.88L; −9.85[1]
8	351.78−0.54		17 26 42.57	−36 09 17.7	2.8; 4[3]
					7.7R; −2.0[4]
9	353.41−0.36		17 30 26.48	−34 41 57.1	11; −19[3]
					18L; −19.7[4]
12	359.981−0.074	SgrA-A	17 45 51.9	−28 59 26.7	16; −28.3[2]
					19; −8.4[2]
					19; −6.8[2]
27	30.82−0.06	W43-Main(3)	18 47 46.9	−01 54 35.2	1.18 ;91.8[5]
29	34.3+0.2	W44	18 53 18.51	01 14 57.6	1.61; 59.2[5]
35	43.167+0.011	W49N	19 10 13.31	09 06 14.3	220L; 15.0[4]
38	49.49−0.387	W51e1/e2	19 23 43.77	14 30 36.3	40; 57.7[2]
		W51Main/S			86R; 58.1[4]
					88.31R; 58.17[1]
					38.29L; 56.98[1]

[1] [17]; [2] [25]; [3] [40]; [4] [9]; [5] [20].

where

$$C_i = \frac{8\pi k\nu \sum g_i}{hc^2 A_{ul} g_u},$$

where A_{ul} is the Einstein coefficient for the ul transition, $\sum g_i$ is the sum of the statistical weights of the levels of the OH ground state, and g_u is the statistical weight of the upper level of the transition. For the transition at 1720 MHz, $C_i = 1.95 \times 10^{15}$ cm^{-2}.

The beam-averaged OH column density for a transition frequency of 1720 MHz is estimated as

$$\langle N_{\rm OH}\rangle = 1.95 \times 10^{15}\ {\rm cm}^{-2} \frac{T_{ex}}{T_{ex} - T_{CMB}} \int \frac{T_A}{\eta} dv.$$

Herw, angular brackets indicate that the density in the regions not completely filling the beam could be higher. The main assumption in calculations using these formulas is that the OH regions are optically thin. We adopted the excitation temperature T_{ex} to be 5 K. It should be borne in mind that for

$$T_{ex} \sim T_{CMB},$$

the ratio

$$\frac{T_{ex}}{T_{ex} - T_{CMB}}$$

can affect the final value of the density very strongly. The results of the calculations are listed in the last column of Table 1.

The OH column densities for the emission lines range from 0.1×10^{16} cm^{-2} (26.508+0.283 Mol 65) to 2.8×10^{18} cm^{-2} (43.167+0.011 W49N). Rejecting

these two extreme cases, we find an average value of N_{OH} for all emission features of about 10^{17} cm^{-2}.

Note that the mean column density N_{OH} in 20 sources (excluding EGOs) found from 37 narrow emission features with linewidths not exceeding 2 km/s is 1.5×10^{17} cm^{-2}. The interval of N_{OH} for absorption lines is from 0.2×10^{16} cm^{-2} (26.508+0.283 Mol 65) to 3.0×10^{17} cm^{-2} (30.69−0.6). Rejecting these two extreme cases, the mean value for the absorption features is 3.6×10^{16} cm^{-2}.

According to earlier observations, the physical conditions at the sites in the ISM where the OH (1720) masers are formed and in the maser condensations emitting MMI lines are fairly similar: the gas cooling a shock has low temperatures (25–125 K), high densities (up to 10^5 cm^{-3}), and OH column densities 10^{17} cm^{-2} [31]. The density of molecular hydrogen in methanol condensations is also about 10^5 cm^{-3} [12, 32]; the typical temperatures can be very low, less than 30 K [33], and the methanol column densities in maser condensations should be higher than in the surrounding medium, where this column density is $>10^{15}$ cm^{-2} [34], more specifically, 10^{16}–10^{17} cm^{-2} [32].

According to interferometric data, the mean size of MMI maser condensations is approximately 1000 AU [35].

Taking into account the probable low temperature of the studied regions, we assume that all hydrogen is molecular. If we use in the density calculation the typical interstellar OH abundance relative to the molecular hydrogen abundance, OH/H$_2$ $\times 10^{-6}$ [28, 36], we find the density for the condensations emitting narrow OH (1720) lines to be $n_{H_2} = 10^7$ cm^{-3}, with the value in the medium producing the absorption lines bing and approximately a factor of ten lower. On the other hand, if we suppose that similar narrow lines could be formed due to the effect of bipolar outflows, the value of X(OH) can increase somewhat, for example, to 10^{-4}–10^{-3} [28]; i.e., narrow emission lines could be formed in a less dense medium, in which n_{H_2} is 10^4–10^5 cm^{-3}.

In any case, it is obvious that the density of material in the medium in which the observed OH (1720) lines are formed is sufficient for MMI masers to arise in the same condensations.

4.4. Observations of EGOs

A catalog of Extended Green Objects (EGOs)—infrared sources extended at 4.5 μm—was recently compiled as part of the *Spitzer* mission [37]. It is supposed that these objects trace bipolar outflows at early stages in the evolution of protostars. In any case, EGOe proved to be a new class of object, in which MMI masers are detected with high probability [38, 39].

We included in our list for the Evpatoria 70-m observations 25 MMI associated with EGOs, of which seven sources were not observed for technical reasons. For 13 EGOs, the result was positive (72% of 18 studied sources), while, for five EGOs (16.59–0.06, 18.67+0.03, 18.89–0.47, 23.965–0.111, and 28.28–0.36), interference prevented us from drawing firm conclusions, although these result were most likely negative.

The MMI/EGO spectra with positive results are included in the 45 sources presented in the figure; the results for the strongest features in the EGOs are listed in Table 1. Negative results are presented in online at http://www.asc.rssi.ru/Lit/LB/online1.pdf.

Eight sources of 13 (10.29–0.13, 10.34–0.143, 11.94–0.62, 19.01–0.03, 19.36–0.03, 25.27–0.43, 39.10+0.491, 49.267–0.337) were initially known as EGOs: MMI emission at 44 GHz was discovered in these objects in the VLA survey [38].

The remaining five sources (14.33–0.64, 34.3+0.2 (W44), 34.403+0.233, 43.04–0.452, and 45.47+0.07) had been known earlier as MMI sources: EGOs from the catalog [37] are identified with them to within 2′. The source 34.3+0.2 (W44) is a supernova remnant; its spectrum has one narrow OH (1720) emission line in both polarizations, with a small absorption in its red wing.

The MMI/OH (1720) spectra toward EGOs have mixed characters, with both emission and absorption lines being observed. These spectra differ somewhat visually from others: in a number of cases, both the emission and absorption line appear more spread out and essentially asymmetric.

We recorded nine narrow emission features with linewidths $\leq$2 km/s. The remaining 14 emission features for EGOs listed in Table 1 are thermal. Taking 34.3+0.2 (W44), which is identified with a supernova remnant, to be atypical we find the average column density for 13 broad EGO emission features without 34.3+0.2 (W44) to be $N_{OH} = 1.3 \times 10^{16}$ cm^{-2}; it is a factor of ten lower for nine narrow features: $N_{OH} = 1.6 \times 10^{15}$ cm^{-2}.

Applying the above considerations to the sizes of the condensations and supposing that EGO regions are definitely associated with bipolar outflows [37], we adopted the OH abundance 10^{-4}–10^{-3} [28]. Thus, we can estimate the density of the medium for the MMI/EGO sources to be $n_{H_2} \simeq 10^2$–10^3 cm^{-3} for the broad lines and $n_{H_2} \simeq 10$–10^2 cm^{-3} for narrow lines.

More detailed EGO data with a larger number of features, including narrow emission lines, are listed in the online Table 3, in the files http://www.asc.rssi.ru/Lit/LB/online5.pdf (EGO spectra) and http://www.asc.rssi.ru/Lit/LB/online6.pdf (Gaussian parameters).

Note again that all the EGO spectra were corrupted by interference, and the observations should be repeated if we wish to obtain a more reliable interpretation.

5. CONCLUSION

Let us summarize our main results.

We have carried out a survey toward 111 Class I methanol masers in the 1720 MHz OH line using the Evpatoria 70-meter radio telescope, with a 9′ beam, a radial velocity resolution of 0.7 km/s, and an average system noise temperature of 35 K.

We obtained 72 spectra without obvious interference, in 27 of which (38%) we observed neither emission nor absorption OH features.

We selected 45 of the most reliable spectra for a statistical analysis. In ten sources, only OH emission lines were observed and in five, only absorption lines, while 30 spectra contained both emission and absorption lines.

Appreciable circular polarization is observed in all spectra.

We have estimated the following mean column densities of OH molecules: $N_{\rm OH} = 1.5 \times 10^{17}$ cm^{-2} for narrow emission features with linewidths not exceeding 2 km/s and $N_{\rm OH} = 3.6 \times 10^{16}$ cm^{-2} for absorption features. Assuming that the size of the studied gas–dust clumps is about 1000 AU (based on interferometric measurements of the sizes of Class I methanol-maser condensations [35]), the density of molecular hydrogen in the condensations emitting narrow OH lines (1720) varies from $n_{\rm H_2} = 10^2$ cm^{-3} to $n_{\rm H_2} = 10^7$ cm^{-3}, depending on whether the region of OH (1720) emission is a fragment of the usual ISM or has been exposed to the front of a bipolar outflow.

The flux densities in narrow features are no less than 100 mJy, and exceed 500 mJy for a considerable number of lines.

These characteristics indicate that the observed OH (1720) lines toward MMI are indeed maser lines, and the observed flux densities indicate the suitability of these sources for VLBI experiments, aimed at determining the sizes and brightness temperatures of the emitting condensations.

Our comparison of the statistical data has demonstrated the following.

OH (1720) maser emission is observed toward 10% of SNRs; i.e., in 20 of 200 SNRs (see [31] and references therein).

According to observations in the Southern hemisphere, OH (1720) maser emission is present toward 11% of SFRs; i.e., in 28 of 200 SFRs [9].

According to observational data for the Northern hemisphere, OH (1720) maser emission is present toward 6% of MMIIs; i.e., toward 6 of 100 SFRs [20].

According to our survey, narrow OH (1720) emission lines are present toward 35% of MMI; i.e., in 25 of 72 MMI for which reliable spectra have been obtained. Thirteen spectra (another 18%) also contain broader OH (1720) emission features at the same velocity as the MMI maser features. These are probably blends that include narrower lines, which could be maser lines.

According to our survey, OH (1720) emission is present toward 72% of MMI discovered toward EGOs; i.e., in 13 of 18 MMI/EGOs. We observe mostly broad OH (1720) emission lines toward MMI associated with EGOs; the mean column density of OH in these does not exceed 10^{16} cm^{-2}, and the density of molecular hydrogen does not exceed 10^2 cm^{-3}, assuming that the size of the condensations is 1000 AU. This may suggest indirectly modest powers for the bipolar outflows, spatial separation of the MMI and OH (1720) condensations, differences in their pumping (e.g., the OH (1720) transition could be excited at a lower density for the gas–dust medium or over a broader density range), or EGO sizes considerably smaller than 1000 AU.

Thus, the main result of this study is the detection of numerous OH (1720) emission lines, many of which could be maser lines, observed in larger numbers toward MMI than toward SNRs, SFRs, and MMIIs, as well as numerous OH (1720) absorption lines, which form narrow asymmetric spectra.

The presence of OH (1720) emission lines can be considered direct evidence for the presence of shocks in the observed regions, most likely arising in the MMI maser condensations during the formation of protostars. The fronts of bipolar outflows from these objects amplify the collisional pumping, which is currently thought to be responsible for both the MMI and OH (1720) lines and spectra containing narrow absorption features in the wings of OH emission lines.

The greatest drawback of these observations is the poor quality of the amplitude calibration. If the flux densities quoted above are overestimated, this will lower the probability that number of the OH sources are masers, though the narrowness of the observed lines supports the idea that they are maser lines.

In any case, most of our results require more detailed studies, due to the complicated situation with interference at the observational site, depending on the time of day and the pointing direction, as well as from an astrophysical point of view.

ACKNOWLEDGMENTS

This work was partially supported by the Russian Foundation for Basic Research (project code 10-02-00147-a), the Basic Research Program of the Division of Physical Sciences of the Russian Academy of Sciences "Active Processes and Stochastic Structures in the Universe," and the Ministry of Education and Science Federal Targeted Program "Scientific and Science-Education Staff of Russia" (state contracts 02.740.11.0251 and 16.740.11.0155). We thank the staff of the Evpatoria Observatory for their help with the observations.

REFERENCES

1. D. Engels and B. Heidmann, in *Why Galaxies Care About AGB Stars II: Shining Examples and Common Inhabitants,* Ed. by F. Kerschbaum, T. Lebzelter, and R. F. Wing, ASP Conf. Ser. **445**, 323 (2011); http://www.hs.uni-hamburg.de/~st2b102/maserdb/vienna10_maser-db.pdf (2010).
2. A. J. Walsh et al., Mon. Not. R. Astron. Soc. **416**, 1764 (2011).
3. M. R. Pestalozzi, V. Minier, and R. Booth, Astron. Astrophys. **432**, 737 (2005).
4. I. E. Val'tts, G. M. Larionov, and O. S. Bayandina, arXiv:1005.3715v3 [astro-ph.GA] (2011); http://www.asc.rssi.ru.MMI (2010).
5. I.Sepulveda, G.Anglada, R.Estalella, et al., http://adsabs.harvard.edu/abs/2010yCat..352790-41S (2011).
6. S. Deguchi, T. Fujii, M. Miyoshi, and J.-I. Nakashima, Publ. Astron. Soc. Japan **54**, 61 (2002).
7. J. E. Lindberg, S. Aalto, F. Costagliola, J.-P. Pérez-Beaupuits, R. Monje, and S. Muller, Astron. Astrophys. **527**, 150 (2011).
8. E. D. Araya, P. Hofner, W. M. Goss, et al., e-Print arXiv:0806.1548v1 [astro-ph] (2008).
9. J. L. Caswell, Mon. Not. R. Astron. Soc. **349**, 99 (2004).
10. J. W. Hewitt, F. Yusef-Zadeh, M. Wardle, et al., Astrophys. J. **652**, 1288 (2006).
11. M. Elitzur, Rev. Mod. Phys. **54**, 1225 (1982).
12. D. M. Cragg, K. P. Johns, and P. D. Godfrey, et al., Mon. Not. R. Astron. Soc. **259**, 203 (1992).
13. A. M. Sobolev and S. Deguchi, Astron. Astrophys. **291**, 569 (1994).
14. A. M. Sobolev, D. M. Cragg, and P. D. Godfrey, Astron. Astrophys. **324**, 211 (1997).
15. R. M. Lees, Astrophys. J. **184**, 763 (1973).
16. M. Elitzur, Astrophys. J. **203**, 124 (1976).
17. A. L. Argon, M. J. Reid, and K. M. Menten, Astrophys. J. **593**, 925 (2003).
18. D. A. Frail, W. M. Goss, E. M. Reynoso, E. B. Giacani, et al., Astron. J. **111**, 1651 (1996).
19. C. L. Brogan, in *Astrophysical Masers and Their Environments*, Ed. by J. M. Chapman and W. A. Baan, Proc. IAU Symp. **242**, 299 (2007).
20. M. Szymczak and E. Gerard, Astron. Astrophys. **414**, 235 (2004).
21. S. Y. Zubrin and V. M. Shulga, in *Proceedings of the 15th Young Scientists' Conference on Astronomy and Space Physics* (Kiev Taras Shivchenko Univ., Kiev, Ukraine, 2008), p. 41.
22. I. D. Litovchenko, A. V. Alakoz, I. E. Val'tts, and G. M. Larionov, Astron. Rep. **55**, 978 (2011).
23. D. A. Frail, Mem. Soc. Astron. Ital. **75**, 282 (2008); arXiv:1108.4137v1 [astro-ph.HE] (2011).
24. Y. M. Pihlström, L. O. Sjouwerman, and V. L. Fish, Astrophys. J. **739**, L21 (2011).
25. B. J. Robinson, W. M. Goss, and R. N. Manchester, Austral. J. Phys. **23**, 363 (1970).
26. W. M. Goss, Astrophys. J. Suppl. Ser. **15**, 131 (1968).
27. I. F. Mirabel, L. F. Rodríguez, and J. Cantó, Astrophys. J. **294**, L39 (1985).
28. F. O. Clark and B. E. Turner, Astron. Astrophys. **376**, 114 (1987).
29. G. M. Larionov and I. E. Val'tts, Astron. Rep. **51**, 756 (2007).
30. H. Liszt and R. Lucas, Astron. Astrophys. **314**, 917 (1996).
31. J. W. Hewitt and F. Yusef-Zadeh, Astrophys. J. **683**, 189 (2008).
32. A. M. Sobolev, A. B. Ostrovskii, M. S. Kirsanova, O. V. Shelemei, M. A. Voronkov, and A. V. Malyshev, *Massive Star Birth: A Crossroads of Astrophysics*, Ed. by R. Cesaroni, M. Felli, E. Churchwell, and M. Walmsley (Cambridge, Cambridge University Press), p. 174–179 (2005).
33. I. E. Val'tts, S. P. Ellingsen, V. I. Slysh, et al., Mon. Not. R. Astron. Soc. **317**, 315 (2000).
34. S. V. Kalenskii, A. M. Dzura, R. S. Booth, A. Winnberg, and A.V. Alakoz, Astron. Astrophys. **321**, 311 (1997).
35. V. I. Slysh, I. E. Val'tts, S. V. Kalenskii, and V. V. Golubev, Astron. Rep. **43**, 785 (1999).
36. B. E. Turner and C. E. Heiles, Astrophys. J. **194**, 525 (1974).
37. C. J. Cyganowski et al., Astron. J. **136**, 2391 (2008).
38. C. J. Cyganowski, C. L. Brogan, T. R. Hunter, and E. Churchwell, Astrophys. J. **702**, 1615 (2009).
39. Chen Xi, S. P. Ellingsen, Shen Zhi-Qiang, et al., Astrophys. J. Suppl. Ser. **196**, Article ID 9 (2011).

Translated by G. Rudnitskii